

Equilibrium Configurations of Homogeneous Fluids in General Relativity

M. Ansorg,¹ T. Fischer,² A. Kleinwächter,² R. Meinel,^{2,*} D. Petroff,² and K. Schöbel²

¹*Center for Gravitational Physics and Geometry, Physics Department,
Penn State, University Park, Pennsylvania 16802, USA*

²*Theoretisch-Physikalisches Institut, University of Jena, Max-Wien-Platz 1, 07743 Jena, Germany*
(Dated: January 23, 2019)

By means of a highly accurate multi-domain pseudo-spectral method, we investigate classes of uniformly rotating, homogeneous and axisymmetric relativistic fluid bodies. In an appropriate parameter diagram, the well-known Maclaurin sequence of rotating fluid spheroids can be divided into segments, each of which is contained within one of the above mentioned classes as one of its Newtonian limits. These segments are separated by the bifurcation points associated with the onset of secular, axisymmetric instability. Further Newtonian sequences branching off at these points also bound the relativistic solutions. Other limits are characterized by mass-shedding and fragmentation, the latter leading to a two-body system and thus a non-homogeneous model. In addition, the first class is also bounded by the non-rotating Schwarzschild spheres and by configurations with infinite central pressure. The second class, which contains the recently studied relativistic Dyson rings, permits an extreme Kerr Black Hole limit. The Newtonian disc limit can only be reached by going through infinitely many of these classes, meaning that one is forced to pass through the aforementioned Newtonian bifurcation points. Only once this limiting process has been consummated, can one proceed again into the relativistic regime and arrive at the analytically known relativistic disc of dust including its extreme Kerr Black Hole limit. In order to explore and understand the totality of the solution space, we also employ recent results regarding the behaviour of the post-Newtonian Maclaurin spheroids.

PACS numbers: 04.20.-q, 04.25.Dm, 04.40.-b, 04.40.Dg, 04.70.-s

I. INTRODUCTION

Self-gravitating bodies of constant density have always played a central role in the physics of gravitation. Contributions that have been most significant to the aspects of this subject that will be relevant to this paper can be divided into (1) work done within Newton's theory of gravitation: Maclaurin [1], Poincaré [2], Dyson [3, 4], Lichtenstein [5], Wong [6] and Eriguchi and Sugimoto [7] and (2) work done within Einstein's theory of gravitation: Schwarzschild [8], Chandrasekhar [9], Bardeen [10] and Butterworth and Ipser [11]. Despite this great investment of effort, it has not yet been possible to explore the whole spectrum of Newtonian, let alone relativistic solutions, even if one restricts oneself to axial symmetry and stationarity. Using sophisticated computer programs, we believe that a great step can be taken toward painting the complete relativistic picture of uniformly rotating, homogeneous and axisymmetric bodies. However, because of the many intricate details in this picture, particularly in the vicinity of limiting configurations, it is necessary to use a computer program robust enough to be able to render such limiting configurations and accurate enough to be able to distinguish between neighbouring solutions of Einstein's equations. For our investigations of homogeneous fluids, we used a code based on multi-domain pseudo-spectral methods [12, 13], which satisfies these

requirements.

It is our intention in this paper to present the relativistic picture in its entirety by describing those parts of it that we have studied explicitly and augmenting them with conjectures as to the rest. The picture that emerges for relativistic homogeneous fluids contains familiar demarcations, which we can use to orient ourselves. It contains, for example, three analytically known solutions: the (inner and outer) Schwarzschild solution [8], the relativistic disc of dust solution [14, 15, 16] as well as the Maclaurin solution [1] as one of its Newtonian limits. This last solution will be a particularly useful point of departure for describing the corresponding relativistic picture. It represents homogeneous, rotating fluid spheroids and, but for a scaling factor, depends for given mass density on only one parameter, thereby allowing one to refer to the "Maclaurin sequence". After introducing some basic equations in Sec. II we thus turn our attention to the Maclaurin solution and its post-Newtonian extension in Sec. III. It turns out that not all relativistic configurations are connected to each other in a continuous way, and it will be useful to introduce the notion of a class of solutions. A given class will be defined to include all configurations of strictly positive mass that are connected continuously to each other. In Sec. IV we review the characteristics of the "first" three classes in detail and provide an overview of the remaining classes. We close with a discussion of the limitations of numerical methods and some thoughts on the completeness of the relativistic picture painted in this paper.

*Electronic address: Meinel@tpi.uni-jena.de

II. EINSTEIN'S FIELD EQUATIONS AND THEIR NUMERICAL SOLUTION

Using Lewis-Papapetrou coordinates, the line element for a stationary, axially symmetric spacetime corresponding to a rigidly rotating perfect fluid configuration can be written in the form

$$ds^2 = e^{2\alpha}(d\varrho^2 + d\zeta^2) + W^2 e^{-2\nu}(d\varphi - \omega dt)^2 - e^{2\nu} dt^2,$$

where the metric functions α , W , ν and ω are functions of ϱ and ζ alone. The boundary of a fluid configuration rotating with the angular velocity Ω obeys the equation

$$e^{2\nu} - W^2(\omega - \Omega)^2 e^{-2\nu} = \text{const.} = (1 + Z_0)^{-2},$$

where Z_0 is the relative redshift observed at infinity of a photon emitted with zero angular momentum from the configuration's surface. Together with regularity requirements along the axis of rotation, $\varrho = 0$, and the asymptotic behaviour, the boundary equation including transition conditions and the field equations themselves form a complete set of equations to be solved (see e.g. [11]). In this paper we choose natural units in which the gravitational constant G and the speed of light c are both equal to one.

This set of equations was solved numerically to very high accuracy using a multi-domain pseudo-spectral method. In the algorithm used, the domains are chosen such that the unknown boundary $\zeta = \zeta_s(\varrho)$ of the configuration always coincides with the boundary between two domains, thus avoiding Gibb's phenomena. The boundary enters into the equations through coordinate transformations, which map the physical domains onto a square. The metric functions and the boundary are represented by a truncated Chebyshev expansion so that the above mentioned set of equations can be reduced to a set of (non-linear) algebraic equations. Further details can be found in [13].

III. THE MACLAURIN SEQUENCE AND ITS BIFURCATION POINTS

Maclaurin showed that for a spheroid (also called an ellipsoid of rotation) of constant density there is a balance of gravitational, centrifugal and pressure forces, leading to equilibrium in Newtonian theory. For a given mass density, this spheroid can be described entirely by specifying the ratio of polar to equatorial radius,

$$A := r_1/r_2, \quad (1)$$

and the focal distance of the ellipse used to generate this ellipsoid of revolution. The focal distance merely provides the scaling of the spheroid and we can use $A \in [0, 1]$ to parameterize the whole solution.

Poincaré [2], Bardeen [10] and Hachisu and Eriguchi [17] all studied points of instability along the Maclaurin

Bifurcation points
$A_1 = 0.17126186 \dots$
$A_2 = 0.11160323 \dots$
$A_3 = 0.08274993 \dots$
$A_4 = 0.06574427 \dots$
$A_5 = 0.05453402 \dots$
$A_6 = 0.04658868 \dots$

TABLE I: Values for the ratio of polar to equatorial radius of the Maclaurin spheroid at the first six bifurcation points associated with the onset of axially symmetric, secular instability.

sequence and the latter three authors were able to show that these correspond to bifurcation points. The bifurcation points that are of particular interest to us here are those marking the onset of the various modes of axially symmetric, secular instability. Values for A at the first few of these can be found in Table I and will be denoted by A_n , ($n = 1, 2, 3, \dots$). There are countably infinitely many such bifurcation points with the accumulation point $A = 0$. Chandrasekhar [9] calculated the post-Newtonian corrections to the Maclaurin spheroids and found that they become singular at the bifurcation point A_1 . Bardeen [10] conjectured that the n^{th} post-Newtonian approximation to the Maclaurin spheroids becomes singular at each of the first n such bifurcation points – a conjecture which was then proved in [18]. As one nears these points, the relativistic parameter used as an expansion parameter in the post-Newtonian series solution is forced to grow arbitrarily small if the solution is to converge at all.

There is strong evidence to support the assumption that this series solution converges in some neighbourhood of the Newtonian solution (see [18]). Assuming such a convergence and restricting ourselves to the convergent region, we found that there exists no continuous transition between two solutions with strictly positive masses (corresponding to strictly positive relativistic parameters) that straddle a bifurcation point. The post-Newtonian Maclaurin spheroids and in particular the specialization to the post-Newtonian disc of dust (see [19]) suggest that the series may in fact converge even for arbitrarily relativistic configurations, which would mean that the “restriction” to the convergent region poses no constraint whatsoever. In terms of the post-Newtonian series, we can parameterize the solution by a relativistic parameter and a second parameter $\xi = \xi(A^M)$ depending only on the radius ratio of the Maclaurin spheroid. In the two-dimensional space spanned by these parameters, the lines $\xi = \xi(A^M = A_n)$ are impermeable barriers, since the post-Newtonian expansion becomes singular anywhere along them.

These barriers allow us to divide our solution space into “classes” of configurations in the following way: We first divide up the Maclaurin sequence into an infinite number of segments with the above mentioned bifurca-

tion points, A_n , separating one segment from the next. These segments can be numbered (or named) starting, for example, from $A = 1$. We can then identify uniquely any configuration of strictly positive mass with a given segment by requiring that the segment be approachable in a continuous way. All those configurations that have been thus associated with segment n make up class n .

As we shall see in the following sections, numerical results lend strong support to the idea that such impermeable barriers as were mentioned above exist and that the definition of a class is thereby justified. In particular, we shall see that it is possible to place ourselves at one of the end-points of a Maclaurin segment and move off the Maclaurin sequence along other well-defined boundaries until we land again on the Maclaurin segment at the second end-point. Neighbouring classes have only this one point as a common boundary.

IV. THE RELATIVISTIC CLASSES

A. Class I: The Generalized Schwarzschild Class

The first class of configurations that will be discussed in this paper was explored extensively in [20]. Here we shall give a brief overview of it, paying particular attention to its defining boundaries.

For a given constant mass density, μ , a stationary, axisymmetric, rigidly rotating relativistic fluid depends on two parameters. A limiting configuration, i.e. one that possesses a physical property representing a boundary, is specified by fixing a corresponding parameter, meaning that it depends on only one further parameter. It is therefore possible to refer to a boundary sequence and identify the end-points of this sequence uniquely with respect to the second parameter.

Clearly the static boundary is marked by the specification $A = 1$. (Note that we also use the radius ratio as defined in Eq. (1) in the relativistic context, where r_1 and r_2 are now coordinate radii.) Static configurations are described by the analytic Schwarzschild solution, which can be parameterized by their central pressure, p_c . Starting from the static end of the Maclaurin sequence ($A = 1, p_c = 0$), let us increase the central pressure until it becomes infinite. This sequence corresponds to a mere point in the lower right corner of Fig. 1 and to the segment from (a) to (b) in the schematic diagram of Fig. 4. Configurations with infinite central pressure are also clearly boundary configurations. We can parameterize these by the normalized angular velocity and follow the sequence from the static limit (where the angular velocity is of course zero) up to its maximal value marked by a mass-shedding limit ((b) to (c) in Fig. 4). Configurations at the mass-shedding limit rotate with an angular velocity equal to that of a test mass rotating at the equator on a circular orbit. They exhibit a cusp at the equatorial rim and are thus easy to identify by the geometry of their surface. We define a mass-shedding

parameter β as in [13] by

$$\beta := -\frac{r_2}{r_1^2} \lim_{\varrho \rightarrow r_2} \zeta_s \frac{d\zeta_s}{d\varrho},$$

where $\zeta = \zeta_s(\varrho)$ represents the boundary of the configuration (see Section II). The mass-shedding parameter takes on the value $\beta = 0$ in the mass-shedding limit and $\beta = 1$ for Maclaurin spheroids. Fixing the value $\beta = 0$, we proceed along the mass-shedding sequence by reducing the central pressure until we reach the Newtonian limit $p_c = 0$ ((c) to (d)).

We can trace the last part of this sequence in the enlargement in Fig. 1, i.e. follow the red curve as it comes in from the top. This curve crosses the Maclaurin sequence in the parameters plotted there at a value for the radius ratio of $A \approx 0.195$. The two configurations at this cross-over point are however clearly not the same since one is a relativistic star rotating at the mass-shedding limit whereas the other belongs to the Newtonian Maclaurin sequence. In some other parameter diagram these two configurations would correspond to distinct points. This and various other intersections in Fig. 1 are merely a consequence of the fact that the configurations considered in this paper depend on two parameters, but not always in a unique way.

We resume our journey along the boundary curves by following the Newtonian sequence, A_1^+ , from (d) to (e) (parameterized again by $p_c = 0$ for example) by increasing β until we reach the Maclaurin curve at the value $\beta = 1$ and find ourselves precisely at the bifurcation point $A = A_1$. This Newtonian sequence and indeed all Newtonian sequences bifurcating from the Maclaurin sequence at the first ten A_n were studied in [21] in which a depiction of the shape of the configurations along these sequences was also provided.

Except for the Schwarzschild solution itself, we consider all the boundaries in the classes to be open, i.e. the limiting sequences themselves are not considered to belong to a solution class. In the case of the Newtonian limit or the limit of configurations with infinite central pressure, it seems appropriate to exclude such configurations from the physically permissible solutions. In the case of the mass-shedding limit or the two-body limit that will arise in later classes, this choice is a mere matter of convention. The extreme Kerr Black Hole, which will present itself in the next section, is also taken to be an open boundary.

Having circumscribed the generalized Schwarzschild class by specifying its boundary configurations, it is possible to discuss those configurations making up this class. Amongst the most interesting properties of this first class is that there is an upper limit on the attainable mass, which is much higher than that known from the static solution. It is well known that the Schwarzschild solution reaches its maximal mass for a configuration with infinite central pressure. Whereas the gravitational mass is bounded by $M\sqrt{\mu} < 4/(9\sqrt{3}\pi) \approx 0.14477$ in this case, the effects of rotation allow for an increase of roughly

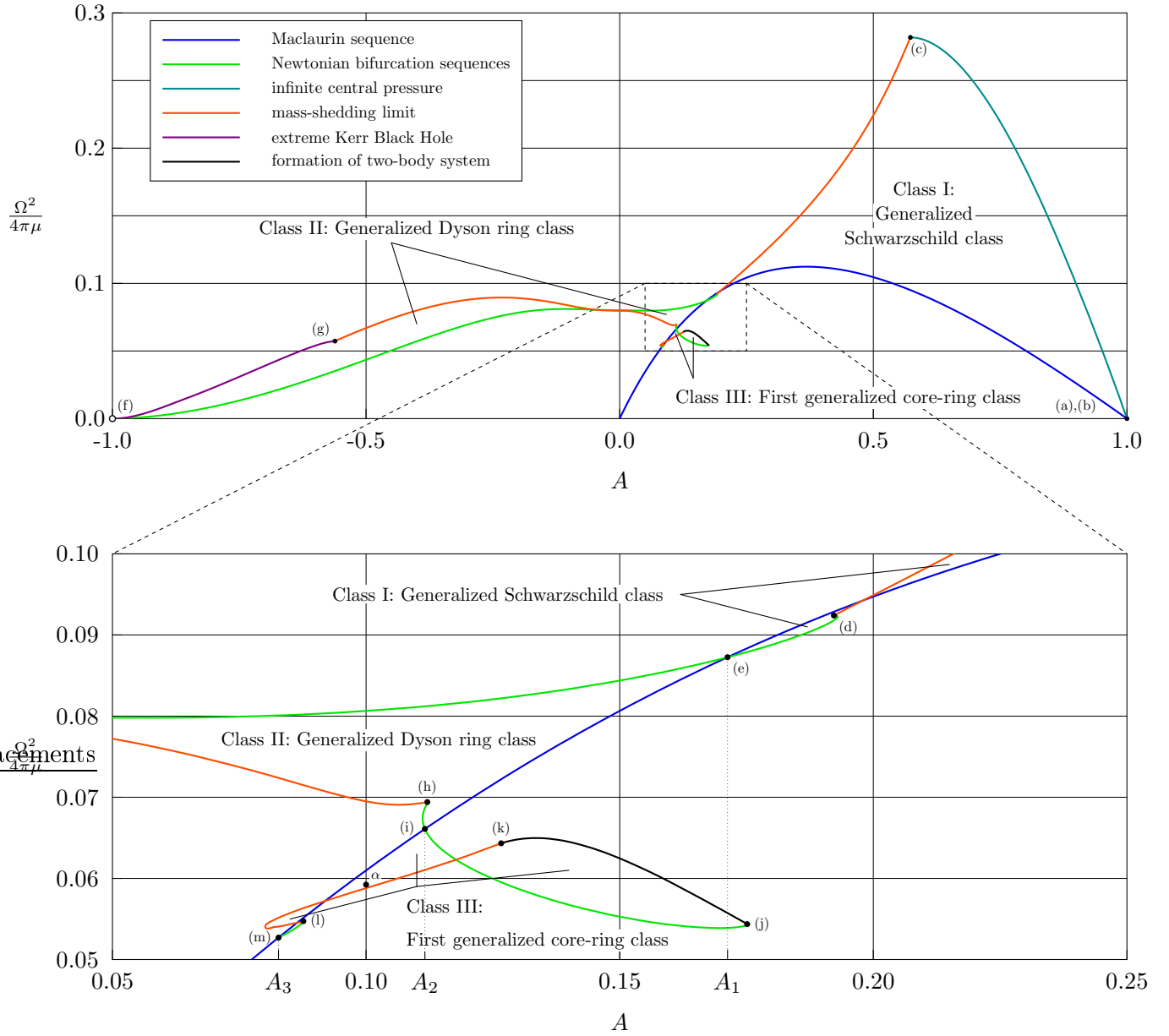


FIG. 1: The square of the normalized angular velocity versus the ratio of radii for the boundary curves of the first three classes.

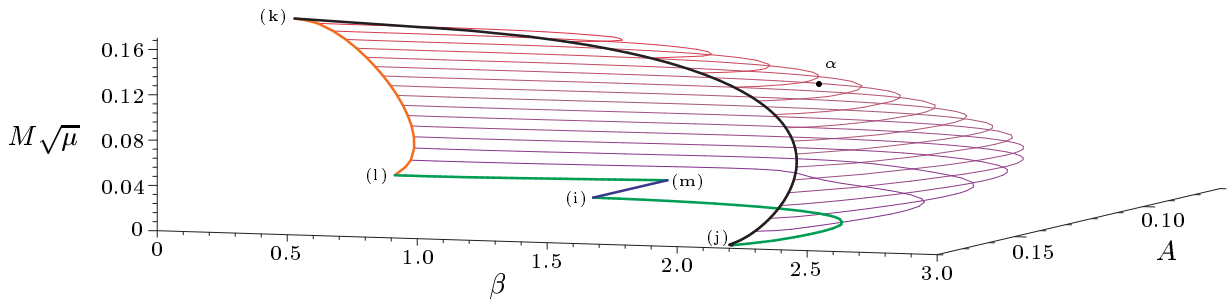


FIG. 2: A three-dimensional parameter diagram depicting all of class III. Lines of constant $M\sqrt{\mu}$ beginning with the Newtonian limit $M\sqrt{\mu} = 0$ (green and blue curves) are drawn in steps of 0.01. The colour coding of the boundary sequences corresponds to that of Fig. 1.

34%. The maximal mass is reached when the sequence with $p_c = \infty$ meets the mass-shedding curve at which point $M\sqrt{\mu} \approx 0.19435$ and many other important physical parameters such as angular velocity, angular momentum and relative redshift become maximal. The reader is referred to [20] for a detailed description of this particularly interesting configuration.

B. Class II: The Generalized Dyson Ring Class

The generalized Dyson ring class was defined and explored in [22]. Here we navigate its boundaries by placing ourselves on the Maclaurin curve at the point $A = A_1$ and proceeding along the sequence A_1^- by decreasing the value of A for $M\sqrt{\mu} = 0$. It turns out that configurations along this sequence pinch together in the centre ($A = 0$), marking the transition from a spheroidal to a toroidal topology. This behaviour was predicted by Bardeen [10], who also correctly surmised that ring configurations are connected to the Maclaurin sequence via the bifurcation point A_1 . Wong [6] as well as Eriguchi and Sugimoto [7] studied such configurations and their connection to the Maclaurin sequence, aspects of which were clarified in [21].

If we define A for toroidal topologies to be the negative ratio of the inner to outer coordinate radius of the ring, i.e.

$$A := \frac{r_1}{r_2} \begin{cases} r_1 = \text{polar radius} & \text{spheroidal} \\ r_2 = \text{equatorial radius} & \\ -r_1 = \text{inner radius} & \text{toroidal} \\ r_2 = \text{outer radius} & \end{cases}$$

then we can continue to decrease its value until we finally arrive at $A = -1$. This limit, about which Dyson expanded his ring solution [3, 4], is problematic however, since the ‘‘corotating Newtonian surface potential’’ tends to minus infinity if the Newtonian mass and the radius r_2 are chosen to be strictly positive and finite. The open circle at (f) in Figs 1 and 4 indicates the subtle and interesting jump to the extreme Kerr Black Hole limit ($Z_0 \rightarrow \infty$).

Although the horizon of the extreme Kerr Black Hole viewed from the ‘‘outside’’ world is a mere point at the origin of the coordinate system used here, there exists an ‘‘inner’’ world (if the limit is taken in rescaled coordinates, see [22, 23]) in which we can increase the value of A until we come to a mass-shedding limit ((f) to (g) in Fig. 4). Following the mass-shedding sequence by decreasing the relative redshift, Z_0 , we cross back over to spheroidal topologies and arrive at the Newtonian mass-shedding configuration for a redshift of zero ((g) to (h)). Following the Newtonian sequence A_2^+ by increasing the value of the mass-shedding parameter, β , we arrive at the bifurcation point A_2 of the Maclaurin sequence and

have completely circumscribed the generalized Dyson-Ring class ((h) to (i)).

The configurations in this class, in contrast to those of the generalized Schwarzschild class, contain no upper bound for the mass. This surprising fact would only be of astrophysical relevance if ring configurations turned out to be stable.¹

Another salient feature of this class is that a continuous transition to an (extreme Kerr) Black Hole is possible. This can be compared to the first class for which configurations reached the boundary of infinite central pressure for finite values of the redshift, which has a global maximum of $Z_0 \approx 7.37825$ in the generalized Schwarzschild class.

C. Class III: The First Generalized Core-Ring Class

As with the first bifurcation point, two Newtonian sequences branch off from the second, and indeed from every bifurcation point. Having arrived at $A = A_2$ from class II by increasing the value of A (cf. Fig. 1), we proceed into the third class along the Newtonian sequence A_2^- by placing ourselves at $A = A_2$ and increasing the value of this ratio further. The configurations take on a central bulge shape, but begin to pinch in toward the outer edge. Finally the indentation pinches together yielding a ring just barely in contact with a central core corresponding to the path from (i) to (j) in Fig. 4 (see Fig. 7 in [21]). Although it would be possible to consider the separation of core and ring, we are not interested here in studying a many-body problem and restrict our attention to single, homogeneous bodies. Thus this ‘‘pinching together’’ marks an end-point of the Newtonian sequence. We can follow the sequence of configurations on the verge of forming a two-body system by allowing the mass to increase. This sequence ends in a mass-shedding limit for the configuration with a global maximum for $M\sqrt{\mu} \approx 0.16$ in this class ((j) to (k) in Fig. 4). Placing ourselves on the mass-shedding sequence, we can allow the mass to decrease until we reach the Newtonian limit ((k) to (l)). From here, the Newtonian sequence can be followed to the point $A = A_3$ by increasing the parameter β ((l) to (m)).

As was discussed in Sec. IV A, two parameters do not necessarily suffice to describe a configuration uniquely. By adding a third dimension, one can resolve such ambiguities. In Fig. 2, a plot of the A , β and $M\sqrt{\mu}$ values for the configurations of Class III can be found. In this plot, a given point on the two-dimensional surface in the three-dimensional parameter space refers only to a single configuration. A projection of the boundary curves onto

¹ We intend to investigate the stability of such configurations in the future, but preliminarily suppose that they are unstable.

	$m = 20$	$m = 30$	$m = 40$
A	0.1	0.1	0.1
$M\sqrt{\mu}$	0.1	0.1	0.1
$M_0\sqrt{\mu}$	0.1093062	0.10930610	0.109306099
$J\mu$	0.01483899	0.014838966	0.0148389661
Z_0	0.4921657	0.49216554	0.492165525
$\Omega/\sqrt{\mu}$	0.8627113	0.86271067	0.862710640

TABLE II: Values for dimensionless physical quantities for an exemplary configuration in Class III with increasing order, m (see [13]), of the numerical approximation. The position of this configuration in Figs 1 and 2 is marked by the letter α .

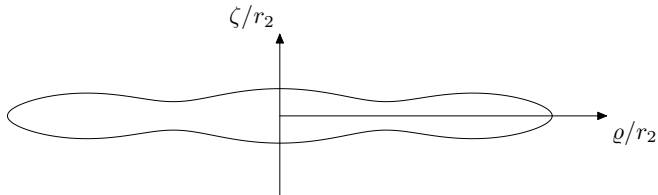


FIG. 3: The meridional cross-section of the boundary of the Class III configuration described in Table II.

the A - β plane would yield a picture of similar complexity to the depiction of class III in Fig. 1. The colours are meant to aid in disentangling the relationship between the various curves as are the letters, which correspond to those of Fig. 4.

An example of various physical parameters for a configuration with the prescribed values $A = 0.1$, $M\sqrt{\mu} = 0.1$ can be found in Table II. The shape of the boundary of this configuration in meridional cross-section is shown in Fig. 3.

D. The Further Classes

As one moves to higher and higher classes, the configurations tend to grow more disc-like. The distance from the Maclaurin curve in the parameters of Fig. 1 grows small although the shapes of the configurations deviate significantly from a spheroid. We term the odd classes, beginning with the third, “core-ring” classes because the configurations on the verge of forming a two-body system contain a central body with a surrounding ring. The central body will itself grow flat in shape and corrugated in appearance as one moves to higher classes. Beginning with the fourth class, the even ones, on the other hand, tend to grow concave at the centre as they “emerge” from the bifurcation points. They then pinch together at the centre and proceed into the toroidal region in which A is negative. Here too, the ring configurations grow flat and corrugated as one moves to higher classes. The corrugations become more pronounced until finally one of them (presumably the outermost) pinches together, whence the name “two-ring” classes for such

configurations. The number of corrugations of the Newtonian sequences is described in [21]. There it was shown at least up to A_{10} that the two Newtonian sequences bifurcating from each A_n end in a mass-shedding limit and a two-body configuration respectively. We assume that this holds for all the bifurcation points. Emanating from the two bifurcation points associated with a given class are two Newtonian sequences, the one ending in a mass-shedding limit and the other in a two-body system. Insofar as the Black Hole limit and that of infinite central pressure are precluded from the higher classes (as indicated by our numerical investigations), the two endpoints of the Newtonian sequences are connected by a mass-shedding and a two-body sequence. The point at which these two configurations meet most likely marks the configuration with the greatest mass for that class.

This overview of the higher classes is based on extrapolation from the first four classes, which were explored exhaustively, the first ten Newtonian bifurcation sequences as well as the behaviour of the post-Newtonian approximation at an arbitrary bifurcation point A_n . As such it cannot be considered absolutely certain, but it certainly rests on firm ground.

In Fig. 4, the classes are depicted schematically. As in this depiction, two neighbouring classes have only the bifurcation point along the Maclaurin sequence in common. The first two classes are atypical in that the first contains the static boundary sequence and one with infinite central pressure and the second contains a sequence of infinite redshift (extreme Kerr Black Hole sequence).

The definition of the classes given in Section III relies on the fact that neighbouring classes have only the bifurcation point along the Maclaurin sequence A_n as a common boundary. As was already mentioned, the post-Newtonian approximation strongly suggests that any sequence of constant, strictly positive mass, parameterized by β and A for example, will be deflected away from the singular point $r_1/r_2 = A_n$ and “back into” the original class. This is exactly what is observed numerically.

In Fig. 5, β versus A values are plotted for sequences of constant mass. Numerical investigations show that sequences belonging to different classes are completely disjoint although the gap in the vicinity of a given A_n grows small for decreasing mass and approaches the point $(A_n, 1)$. This feature, which was already conjectured by Bardeen [10], can be seen distinctly in the figure around A_1 . Such a gap was observed numerically around A_2 and A_3 as well. A comparison with Fig. 2 shows why the curve $M\sqrt{\mu} = 0.01$ of that plot deviates so markedly from the Newtonian boundary curves. If one were to plot such contour lines for increasingly diminishing values of $M\sqrt{\mu}$, the tendency to approach the Newtonian limit would be evident.

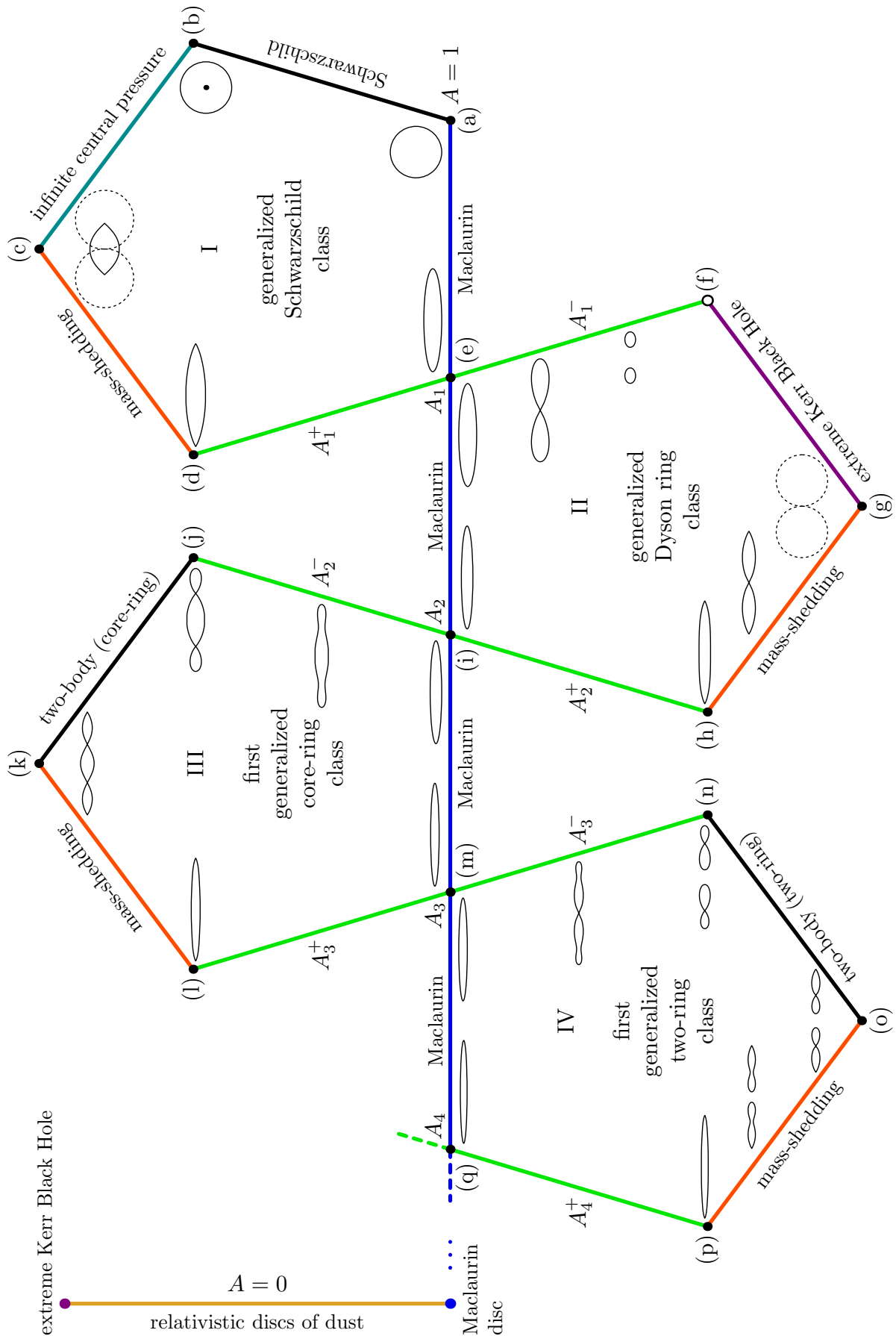


FIG. 4: A schematic portrayal of the classes and their boundaries. A depiction of the surface of configurations in meridional cross-section is provided for configurations at the intersection point of two boundary sequences (except for the point (f), see Sec. IV B). In addition, various surfaces are shown to help illustrate the transition from one corner to the next. Whenever ergo-regions arise, they are depicted by dashed lines (hence the dot in the centre of the configuration located at (b)).

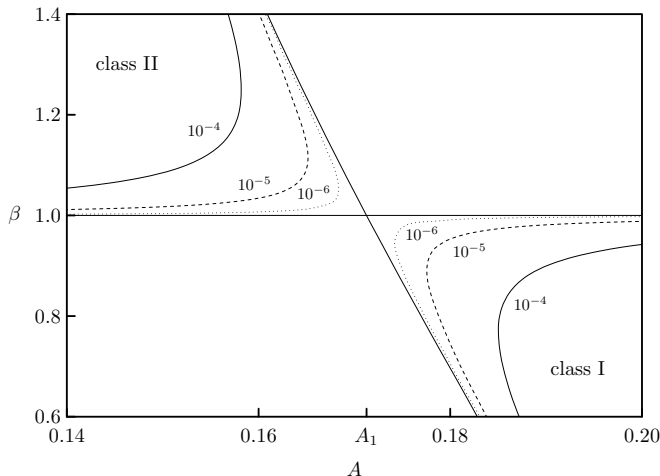


FIG. 5: The relationship of β to A for sequences of constant mass in the vicinity of the bifurcation point associated with A_1 (the point (e), cf. Fig. 4). The solid line represents configurations with $M\sqrt{\mu} = 10^{-4}$, the dashed line with $M\sqrt{\mu} = 10^{-5}$ and the dotted line with $M\sqrt{\mu} = 10^{-6}$. The thin horizontal line represents the Maclaurin sequence and the thin line crossing it is made up of the Newtonian bifurcation sequences A_1^+ and A_1^- (see Fig. 4). Note the gap between the sequences of class I and class II.

V. DISCUSSION

Numerical evidence suggests that as one proceeds to flatter configurations (higher classes), the departure from the Newtonian sequence grows small. This is reflected in the fact that boundaries associated with highly relativistic attributes such as infinite central pressure or the transition to a Black Hole are presumably absent from all classes upwards of class II and is a result of excluding many-body configurations.² If one were to abandon this restriction and choose some (arbitrary) relationship for the rotation of the various segments, then it would again be possible to reach “relativistic boundaries” most likely. With this restriction in place, however, the only path to

the disc of dust passes through an infinite number of bifurcation points and sees the configurations growing ever flatter and more and more corrugated until one lands necessarily at the Newtonian Maclaurin disc. Only once this limit has been reached can one proceed again into the relativistic regime, i.e. the relativistic disc of dust [15] and indeed reach the extreme Kerr Black Hole. This picture reinforces Bardeen’s speculations in [10], who wrote that the singularities in the post-Newtonian expansion at the bifurcation points “may forbid the existence of any highly relativistic, highly flattened, uniformly rotating configurations which are simply connected.” He went on to conclude that the “only acceptable model of an infinitesimally thin, uniformly rotating disk in general relativity may be one that is made up of an infinite number of disjoint rings.”

The complicated and highly non-linear set of equations describing axially symmetric, stationary, uniformly rotating fluids of constant density can only be solved approximately or numerically. As such, it is difficult to find strict results describing the solution set. It is conceivable, for example, that there exist solutions to these equations that possess no Newtonian limit (and must thus be disconnected from the classes of solutions introduced here). It is also conceivable that Newtonian solutions exist that have not yet been found, but serve as limits to relativistic solutions.

Although our numerical considerations do not preclude the possibility of the existence of undiscovered solutions, we presume to conjecture that the classes presented here cover the entire solution space. Attempts to prove or disprove this conjecture are bound to lead to innovative insights into the nature of Einstein’s equations and novel methods for probing their structure.

Acknowledgments

This research was funded in part by the Deutsche Forschungsgemeinschaft (SFB/TR7-B1).

² Furthermore, we did not find ergospheres for these higher classes (beyond class II).

-
- [1] C. Maclaurin, *A Treatise on Fluxions. In two volumes* (William Baynes & William Davis, London, 1801), 2nd ed.
 - [2] H. Poincaré, *Acta mathematica* **7**, 259 (1885).
 - [3] F. Dyson, *Philos. Trans. R. Soc. London, Ser. A* **184**, 43 (1892).
 - [4] F. Dyson, *Philos. Trans. R. Soc. London, Ser. A* **184**, 1041 (1893).
 - [5] L. Lichtenstein, *Gleichgewichtsfiguren Rotierender Flüssigkeiten* (Springer, Berlin, 1933).
 - [6] C. Wong, *Astrophys. J.* **190**, 675 (1974).
 - [7] Y. Eriguchi and D. Sugimoto, *Prog. Theor. Phys.* **65**, 1870 (1981).
 - [8] K. Schwarzschild, *Sitzungsberichte der Königlich Preussischen Akademie der Wissenschaften* **1**, 424 (1916).
 - [9] S. Chandrasekhar, *Astrophys. J.* **147**, 334 (1967).
 - [10] J. Bardeen, *Astrophys. J.* **167**, 425 (1971).
 - [11] E. Butterworth and J. Ipser, *Astrophys. J.* **204**, 200 (1976).
 - [12] M. Ansorg, A. Kleinwächter, and R. Meinel, *Astron. As-*

- trophys. **381**, L49 (2002).
- [13] M. Ansorg, A. Kleinwächter, and R. Meinel, *Astron. Astrophys.* **405**, 711 (2003).
- [14] J. Bardeen and R. Wagoner, *Astrophys. J.* **167**, 359 (1971).
- [15] G. Neugebauer and R. Meinel, *Phys. Rev. Lett.* **75**, 3046 (1995).
- [16] G. Neugebauer and R. Meinel, *J. Math. Phys.* **44**, 3407 (2003).
- [17] I. Hachisu and Y. Eriguchi, *Publ. Astron. Soc. Japan* **36**, 497 (1984).
- [18] D. Petroff, *Phys. Rev. D* **68**, 104029 (2003).
- [19] D. Petroff and R. Meinel, *Phys. Rev. D* **63**, 064012 (2001).
- [20] K. Schöbel and M. Ansorg, *Astron. Astrophys.* **405**, 405 (2003).
- [21] M. Ansorg, A. Kleinwächter, and R. Meinel, *Mon. Not. R. Astron. Soc.* **339**, 515 (2003).
- [22] M. Ansorg, A. Kleinwächter, and R. Meinel, *Astrophys. J. Lett.* **582**, L87 (2003).
- [23] R. Meinel, *Ann. Phys. (Leipzig)* **11**, 509 (2002).